Article

Automated iterative Csp^3–C bond formation

https://doi.org/10.1038/s41586-022-04491-w

Received: 20 September 2021

Accepted: 28 January 2022

Published online: 8 February 2022

Check for updates

Daniel J. Blair[1]✉, Sriyankari Chitti[1], Melanie Trobe[1], David M. Kostyra[1], Hannah M. S. Haley[1], Richard L. Hansen[2], Steve G. Ballmer[2], Toby J. Woods[3], Wesley Wang[1], Vikram Mubayi[1], Michael J. Schmidt[1], Robert W. Pipal[1], Greg. F. Morehouse[1], Andrea M. E. Palazzolo Ray[1], Danielle L. Gray[3], Adrian L. Gill[2] & Martin D. Burke[1,4,5,6]✉

Fully automated synthetic chemistry would substantially change the field by providing broad on-demand access to small molecules. However, the reactions that can be run autonomously are still limited. Automating the stereospecific assembly of Csp^3–C bonds would expand access to many important types of functional organic molecules[1]. Previously, methyliminodiacetic acid (MIDA) boronates were used to orchestrate the formation of Csp^2–Csp^2 bonds and were effective building blocks for automating the synthesis of many small molecules[2], but they are incompatible with stereospecific Csp^3–Csp^2 and Csp^3–Csp^3 bond-forming reactions[3–10]. Here we report that hyperconjugative and steric tuning provide a new class of tetramethyl *N*-methyliminodiacetic acid (TIDA) boronates that are stable to these conditions. Charge density analysis[11–13] revealed that redistribution of electron density increases covalency of the N–B bond and thereby attenuates its hydrolysis. Complementary steric shielding of carbonyl π-faces decreases reactivity towards nucleophilic reagents. The unique features of the iminodiacetic acid cage[2], which are essential for generalized automated synthesis, are retained by TIDA boronates. This enabled Csp^3 boronate building blocks to be assembled using automated synthesis, including the preparation of natural products through automated stereospecific Csp^3–Csp^2 and Csp^3–Csp^3 bond formation. These findings will enable increasingly complex Csp^3-rich small molecules to be accessed via automated assembly.

Automated iterative assembly of chemical building blocks broadens access to innovation at the molecular scale[1]. Methods for reversibly attenuating the reactivity of the functional group handles used to link such blocks are critical for these platforms. For unsaturated (Csp^2-rich) organic small molecules, such lego-like assembly in automated and/or manual fashion has been achieved by many different research groups worldwide using *N*-methyliminodiacetic acid (MIDA) boronates[2,14–16], which are compatible with anhydrous basic Csp^2 cross-coupling conditions (Fig. 1a). An important advantage of MIDA relative to other ligands that attenuate boronic acid reactivity (for example, 1,8-diaminonaphthalene, anthranilamide, ethanolamine, fluoride)[17] is that MIDA boronates display a tuneable affinity for silica gel, which permits generalized automated purification[2]. This unique feature enabled assembly of 14 distinct classes of small organic molecules using one automated process[2].

Important areas of chemical space remain inaccessible with this first-generation platform, particularly for molecules rich in non-planar and potentially stereogenic sp^3-hybridized carbon atoms (Csp^3). This represents a substantial limitation, because Csp^3-rich molecules constitute some of the most notable natural products, medicines[18], biological probes and functional materials[19]. An important goal is thus to expand automated modular synthesis to include Csp^3-rich small molecules.

Many recent breakthroughs in stereospecific formation of Csp^3–C bonds through Suzuki–Miyaura couplings[6,7] and 1,2-metallate rearrangements[8–10] stand to enable advances in this direction (Fig. 1b). However, most of these reactions require either aqueous basic conditions that hydrolyse MIDA boronates, or nucleophilic reagents that react with MIDA boronates (Fig. 1c). In both cases loss of the MIDA protecting group will lead to uncontrolled couplings and form complex mixtures and/or oligomeric products. We thus sought hyperstable boronates to enable lego-like small-molecule synthesis via iterative Csp^3–C bond formation.

Identifying a hyperstable boronate

Mechanistic studies on MIDA boronate hydrolysis provided a foundation for developing hyperstabilized variants[20]. There are two mechanisms for MIDA boronate hydrolysis. The first involves frustrated Lewis pair-like activation of water by the dative N–B bond. The second mechanism involves ester hydrolysis-like cleavage of a MIDA carbonyl (C=O) group by hydroxide. Steric shielding would probably protect the carbonyl carbons from hydroxide and nucleophiles, yet steric effects are known to activate frustrated Lewis pair behaviour of N–B bonds[21–23]. Although hydrolysis studies of MIDA boronates[20] indicated electronic tuning of the N–B bond could be achieved via modifying the organic group attached to boron, we required a building block-independent solution. So, at the outset it was unclear whether steric or electronic effects could be leveraged to create a more stable ligand.

Using [^{18}O]water to probe the hydrolysis of MIDA boronate **1a**[20], we first established the N–B bond as the primary hydrolysis mechanism

[1]Roger Adams Laboratory, School of Chemical Sciences, University of Illinois at Urbana-Champaign, Urbana, IL, USA. [2]Department of Chemistry, REVOLUTION Medicines, Inc., Redwood City, CA, USA. [3]George L. Clark X-Ray Facility and 3M Materials Laboratory, University of Illinois at Urbana-Champaign, Urbana, IL, USA. [4]Carle Illinois College of Medicine, Urbana, IL, USA. [5]Arnold and Mabel Beckman Institute, University of Illinois at Urbana-Champaign, Urbana, IL, USA. [6]Department of Biochemistry, University of Illinois at Urbana-Champaign, Urbana, IL, USA. ✉e-mail: danielb@illinois.edu; mdburke@illinois.edu

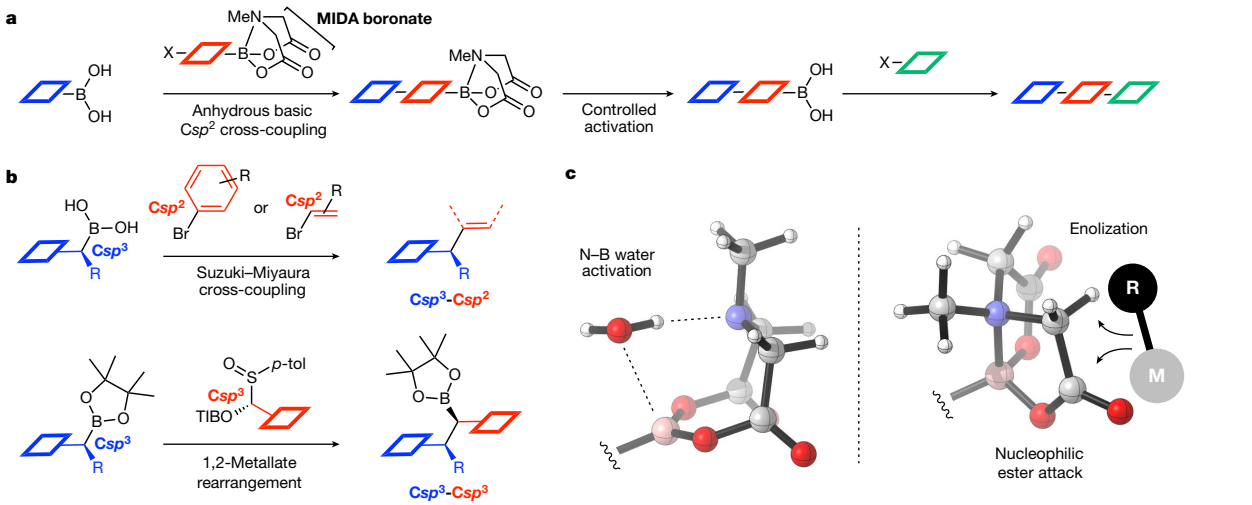

Fig. 1 | Lego-like chemical synthesis. a, Iterative chemical synthesis. Automated synthesis is achieved using bifunctional MIDA boronate building blocks. Controlled removal of MIDA enables iterative synthesis. **b**, Leading Csp^3–C bond-formation methods. Csp^3–Csp^2 cross-coupling of organoboranes is typically achieved under aqueous basic conditions. 1,2-Metallate rearrangements of boronic esters achieve Csp^3–Csp^3 bond formation by using Grignard and organolithium reagents. **c**, Sensitivity of MIDA boronates to Csp^3–C bond-forming conditions. Conditions permissive of Csp^3–C bond formation cleave MIDA boronates and are therefore incompatible with automated lego-like synthesis. *p*-tol, *para*-toluene; TIBO, 2,4,6-triisopropylbenzoate.

under aqueous basic Csp^3–Csp^2 Suzuki–Miyaura coupling conditions (THF/H_2O, K_2CO_3, 60 °C) (Fig. 2a). We thus required a MIDA derivative that could suppress the frustrated Lewis pair like reactivity of the N–B bond. To better understand this behaviour, we used ^{1}H NMR to study the stability of a range of substituted MIDA derivatives (**1b**, **3**–**9**) in deuterated solvent (THF-d_8/D_2O, K_2CO_3, 60 °C) (Fig. 2b).

Consistent with earlier precedent[22,23], bulky groups on nitrogen (Fig. 2b **3**–**5** and Supplementary Fig. 2a) increased the rate of hydrolysis relative to MIDA (**1b**), probably increasing N–B frustrated Lewis pair-like behaviour. Remarkably, appending two *n*-butyl groups (**6**) to the iminodiacetic acid backbone caused almost no change in hydrolysis rate relative to MIDA (**1b**). Reducing the size of these substituents to ethyl groups (**7**) and methyl groups (**8**) provided impressive stabilization. Finally, we prepared a boronate derived from a highly sterically hindered tetramethylated variant of *N*-methyliminodiacetic acid **9** (TIDA) and, surprisingly, found it was highly stable under aqueous basic Csp^3-Csp^2 cross-coupling conditions, with more than 99% remaining after 6 h (Fig. 2b).

Additional hydrolysis studies of TIDA boronate **21** under these conditions in protic solvent (Supplementary Figs. 3, 4), [^{18}O] labelling (Supplementary Fig. 5) and neutral hydrolysis (Supplementary Fig. 6) indicated that TIDA boronates were cleaved via N–B bond water activation. The hyperstable TIDA boronate was retained during Csp^3-Csp^2 Suzuki–Miyaura reaction between Csp^3 boronate **10** and bifunctional halo-TIDA boronate **11b** to provide **12**, whereas MIDA boronate **11a** (Fig. 2c) and related *N*-2-benzyloxycyclopentyliminodiacetic acid (BIDA) boronate **SI-14** (Supplementary Fig. 2b) gave no desired product.

Encouraged by these results, we tested the stability of TIDA boronates to *i*PrMgCl·LiCl, which promotes stereospecific Csp^3–Csp^3 bond-forming 1,2-metallate rearrangements[10] (Fig. 2d). TIDA boronate **14b** resists cleavage by *i*PrMgCl·LiCl to form the target product **15** in high yield, whereas MIDA boronate **14a** is cleaved under these conditions. Remarkably, TIDA boronates even tolerated highly reactive *t*BuLi, enabling the formation of **18** and **19** with excellent diastereocontrol (Fig. 2e). Providing an additional practical advantage, our bifunctional sulfoxide[10] TIDA boronate building blocks (that is, **14**, **16** and **17**) are easily handled, bench-stable solids (Supplementary Fig. 1).

X-ray crystallographic studies

The stability of **9** towards aqueous base is surprising considering the strong precedent for increased reactivity of frustrated Lewis pairs derived from tetramethylpiperidine[21]. Hints at the origin of this stability were found on X-ray crystallographic analysis of single crystals of MIDA boronate **1c** (Fig. 3a, inset) and TIDA boronate **20** (Fig. 3b, inset), which revealed a torsional shift of greater than 10° along the N–B axis in TIDA **20** relative to MIDA **1c**.

Torsional effects can substantially influence[24] the magnitude of hyperconjugative stabilization (that is, staggered versus eclipsed ethane[25]). Torsional shifts in **20** bring three donor N–C bonds nearly antiperiplanar to three acceptor bonds (two B–O bonds and one B–C bond), potentially elevating hyperconjugation across the N–B bond. Backbone methylation would probably increase N–C donor ability, and internal angle compression in **20** (approximately 5°) suggests thermodynamic Thorpe–Ingold effects make the framework more rigid (Extended Data Fig. 1a). Both effects probably reinforce putative hyperconjugation across the N–B bond in **20**. We thus questioned whether stabilizing hyperconjugative interactions across the N–B bond in TIDA boronates drives a reduction in the rate of N–B hydrolysis.

Electron distribution analysis

To probe electronic effects experimentally, we performed quantum theory of atoms in molecules (QTAIM)-based charge density analysis[11–13] on X-ray crystal structures of MIDA boronate **1c** and TIDA boronate **20**. Multiple lines of evidence revealed that the dramatic reduction in hydrolysis for TIDA boronates is attributable to hyperconjugation-mediated redistribution of electron density that increases the covalency of the N–B bond.

Topology maps of crystallographically determined bonding electron density, ρ, demonstrated electron redistribution across planar slices spanning the iminodiacetic acid rings of MIDA **1c** and TIDA **20** (Fig. 3a, b). Notable features of TIDA **20** included increased electron density spanning the N–B interatomic space (Fig. 3b and Extended Data Fig. 2j), and formation of a contiguous ring of electron density around the iminodiacetic acid cage (Fig. 3b). The stabilizing nature of electronic redistribution with the N–B bond of TIDA **20** was supported

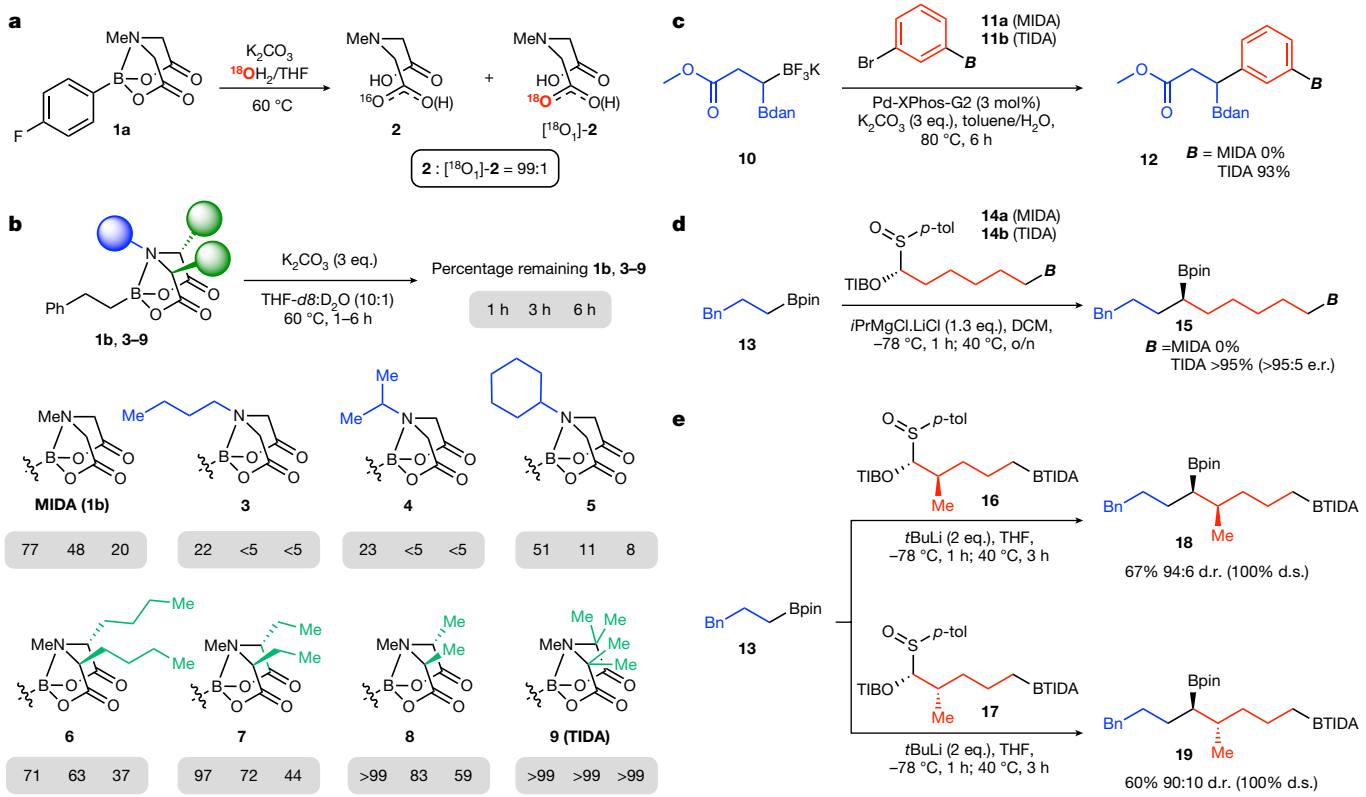

Fig. 2 | TIDA boronates are exceptionally stable towards hydrolytic and nucleophilic cleavage. a, MIDA boronate **1a** is hydrolysed via N–B bond-mediated water activation under standard stereospecific Csp^3 coupling conditions. **b**, Modifications of the MIDA ligand yield varying degrees of stability for the corresponding iminodiacetic acid boronates under common aqueous basic stereospecific Csp^3–Csp^2 coupling conditions. TIDA boronate **9** is exceptionally stable. eq., equivalents . **c**, TIDA boronates resist hydrolysis during Csp^3–Csp^2 Suzuki–Miyaura coupling with **10**, whereas MIDA boronates are completely hydrolysed. **d**, TIDA boronates were stable to the Grignard reagent *i*PrMgCl·LiCl enabling Csp^3–Csp^3 bond-forming 1,2-metallate rearrangements, whereas MIDA boronates were cleaved under these conditions. **e**, The remarkable stability of TIDA boronates extends to *t*BuLi. Diastereospecificity (d.s.) = (final diastereoisomeric ratio/initial diastereoisomeric ratio) × 100. dan, 1,8-diaminonaphthalene; pin, pinacolato.

by a negative Laplacian of electron density $\nabla^2\rho(r)$ at boron and nitrogen valence shell charge concentrations (Extended Data Fig. 3j). TIDA **20** therefore possesses an N–B bond of substantially increased covalent character.

Elongation of nitrogen-attached donor bonds and boron-attached acceptor bonds (Extended Data Fig. 1b), consistent with previous studies of anomeric[26] and gauche effects[27], supports threefold hyperconjugation along the N–B linkage. Anticipated increased π-character manifested localized increased ellipticity (ε)[11] (Extended Data Fig. 4c, f, g, j, l, m), and redistributed electron density was supported by changes in $\nabla^2\rho(r)$ (Extended Data Fig. 3e, f, k)[28]. Electrostatic potential maps, reduced polarization of the N–B bond[29] and ^{11}B/^{13}C NMR shifts were also consistent with electron redistribution (Extended Data Fig. 5). Additional stabilizing electronic redistributions were found on examination of ρ, $\nabla^2\rho(r)$ and ε surrounding boron-attached oxygens O1 and O4, which revealed more equal distribution of electron density directed towards boron and the carbonyl carbons for TIDA **20** compared to MIDA **1c** (Extended Data Figs. 2b, c, h, i, 3b, c, h, i, 4c, d, i, j and 6).

Increased electron sharing[30] is consistent with reduced propensity for frustrated Lewis pair activity[31–33], and rationalizes the increased robustness of TIDA boronates towards N–B bond hydrolysis. Remarkably, these stark differences in N–B bond character are contrasted with similar bond lengths (MIDA **1c**: 1.6613(7) Å; TIDA **20**: 1.6632(5) Å).

Steric shielding of TIDA boronates

Crystallographic data for TIDA **20** also indicated that the stability of TIDA boronates towards carbon nucleophiles (*i*PrMgCl·LiCl and *t*BuLi) arises from shielding of all four π-faces of the carbonyls by the attached methyl groups (Fig. 3c and Extended Data Fig. 7a[34]). Comparison with organolithium-stable Beak-type benzoates[35] revealed that **20** mirrors Beak-like shielding interactions via a transannular methyl group spanning the back face of the iminodiacetic acid cage (Extended Data Fig. 7b).

Synthetic utility of TIDA boronates

Reversible ligation is a requirement for deploying TIDA boronates in iterative cross-coupling-based building block assembly. An orthogonal pathway for hydrolysis involving C=O attack (Supplementary Fig. 7 and Extended Data Fig. 8a) enabled TIDA boronates (**21**) to be deprotected to boronic acids (**22**), trifluoroboronate salts (**23**), and boronic esters[36] (**24**, **25**) by simply using aqueous basic or protic conditions at elevated temperature (Fig. 3d).

TIDA boronates retain all other key features of their MIDA boronate counterparts that enabled automated building block-based synthesis[2]: TIDA ligand is accessible on the kg scale (Extended Data Fig. 8b), TIDA boronates are prepared from boronic acids under Dean–Stark conditions or by using a dehydrated form of TIDA (Extended Data Fig. 8c), TIDA boronates are stable to a wide range of common cross-coupling reactions (that is, Stille, Suzuki, Sonogashira, Heck, photochemical; see Extended Data Fig. 9) and chemical transformations (that is, oxidation, reduction, borylation, olefination; see Extended Data Fig. 10). Representative TIDA boronates retain a tuneable affinity for silica gel, being minimally mobilized in Et_2O and rapidly eluted in THF (Extended Data Fig. 8d). This feature enables the TIDA boronate group to act as

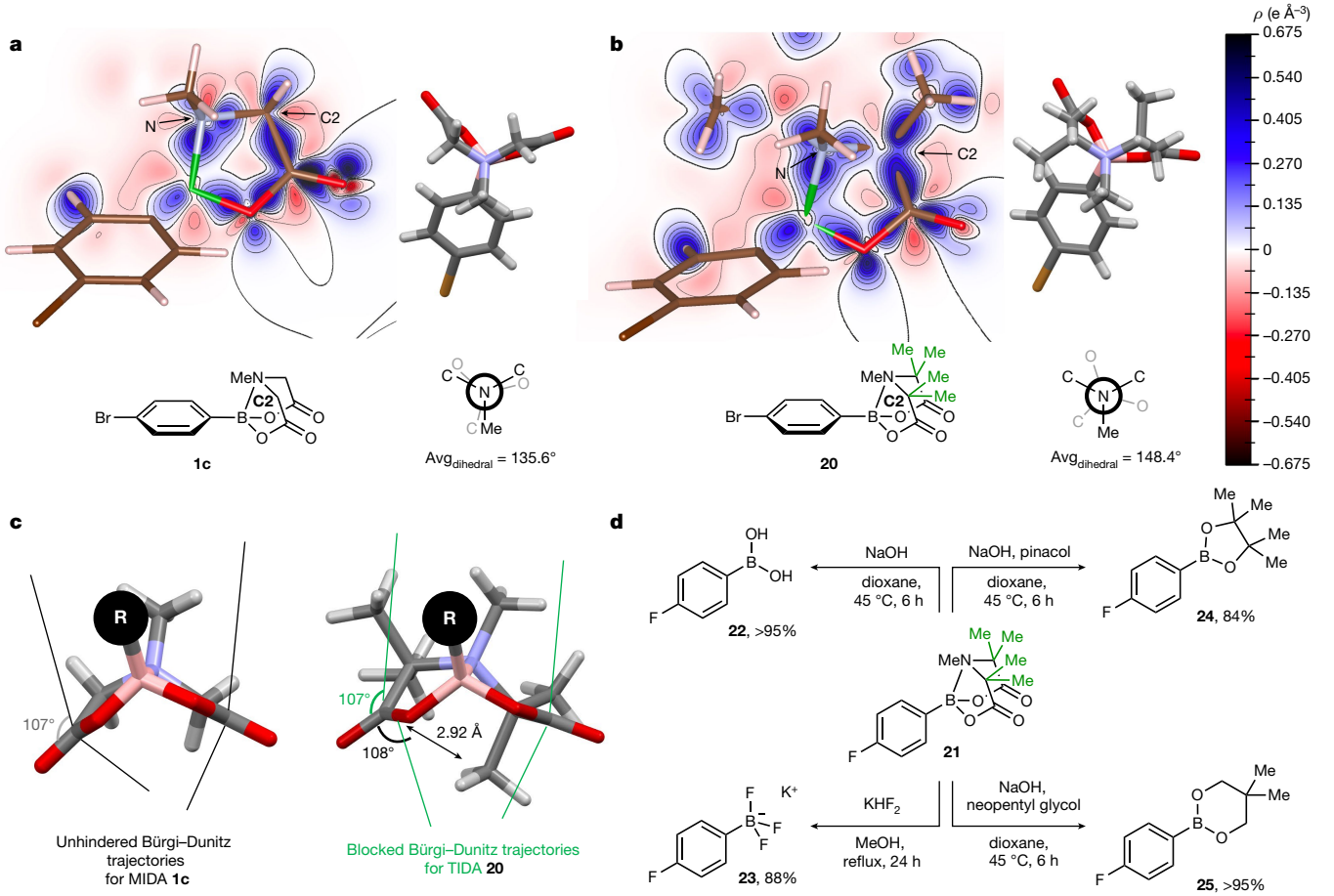

Fig. 3 | Steric and electronic effects collaborate to stabilize TIDA boronates. a, Examination of non-spherical (that is, bonding) electron density (ρ) in the plane of the iminodiacetic acid ring of MIDA boronate **1c**. Contour level 0.0675 e Å^{-3}. Shown inset is the perspective looking down from N to B. **b**, Non-spherical electron density in the plane of the iminodiacetic acid ring of TIDA boronate **12** shows substantial electronic redistribution compared to MIDA boronate **1c**, particularly for the N–B bond. An associated 12° torsional shift increases hyperconjugative interactions along the N–B axis compared to MIDA **1c**. **c**, Comprehensive steric shielding of all four π-faces of TIDA boronates suppresses nucleophilic attack on the carbonyl carbons. **d**, Despite their high stability towards Csp^3 bond-forming reactions, TIDA boronates are easily removed under aqueous or protic conditions at elevated temperatures. Contour plots were generated using VESTA 3 (ref. [42]).

a tag for generalized and automated catch-and-release purification[2]. The heightened stability of TIDA boronates further enabled us to create a self-contained next-generation synthesis machine (Supplementary Figs. 8–11 and 13) to enable automated iterative assembly of Csp^3 boronate building blocks (Fig. 4a, d).

Having established an iterative synthesis platform (Fig. 4a), we investigated a series of stereospecific Csp^3–Csp^2 cross-coupling reactions with bifunctional halo-TIDA boronates (Fig. 4b). Across a range of carbonate-promoted aqueous/protic stereospecific Csp^3 cross-coupling reactions[6,7], MIDA boronates were fully hydrolysed, whereas the corresponding TIDA boronates universally provided the desired products in good yields both in manual and automated formats (**12**, **26**, **27** and **28**). The increased stability of TIDA boronates also permitted use of stronger bases KOH (**31**)[5] and Ag_2O (**30**)[4].

Leveraging automated Csp^3–Csp^2 couplings with TIDA boronates, we targeted a lego-like total synthesis of ieodomycin C[37] (Fig. 4c). Building block **31** (97:3 enantiomeric ration (e.r.)) underwent automated stereospecific Csp^3 cross-coupling with bifunctional TIDA boronate **32** to provide **33** in >95:5 e.r. and 50% isolated yield after automated purification. TIDA boronate enabled functional group interconversion followed by deprotection (**34**), and Suzuki–Miyaura cross-coupling with vinyl halide **35** furnished diene **36** and ieodomycin C after deprotection.

The tolerability of TIDA boronates to *i*PrMgCl·LiCl enabled 1,2-metallate rearrangements to be executed with bifunctional sulfoxide-TIDA boronate building blocks in manual and automated formats (Fig. 4d) to prepare a variety of Csp^3–Csp^3 bonds in excellent yields (Fig. 4e, **15** and **37**-**42**). A triply boron-selective reaction was also achieved in the diastereospecific preparation of **43** and **44**. Csp^2 boronic esters were also effective (**45**, **46**).

Reactivity differences between unhindered/hindered boronic esters[38,39] suggested potential for iteration-enabling kinetic selectivity within Csp^3–Csp^3 bond formation. Accordingly, we investigated the lego-like automated synthesis of macrocyclic antifungal natural product sch725674 (ref. [40]) (Fig. 4f). Demonstrating the advantage of our approach over previous strategies[41] to access sch725674, our bifunctional sulfoxide-TIDA boronate **14b** enabled recursive application of the same assembly chemistries to form Csp^3–Csp^3 bonds. Additionally, the inclusion of a TIDA boronate enabled this entire process of multiple building block assembly via iterative Csp^3–Csp^3 bond formation to be executed in a fully automated and uninterrupted fashion (Supplementary Figs. 14 and 15). *n*-Pentyl pinacol boronic ester **47** was subject to 1,2-metallate rearrangement with sulfoxide-boronate **14b** to afford the target TIDA boronate **48** in high stereocontrol (>95:5 e.r.). Automated deprotection to the corresponding pinacol boronic ester **49** was followed by automated boronic ester-selective reaction with sulfoxide

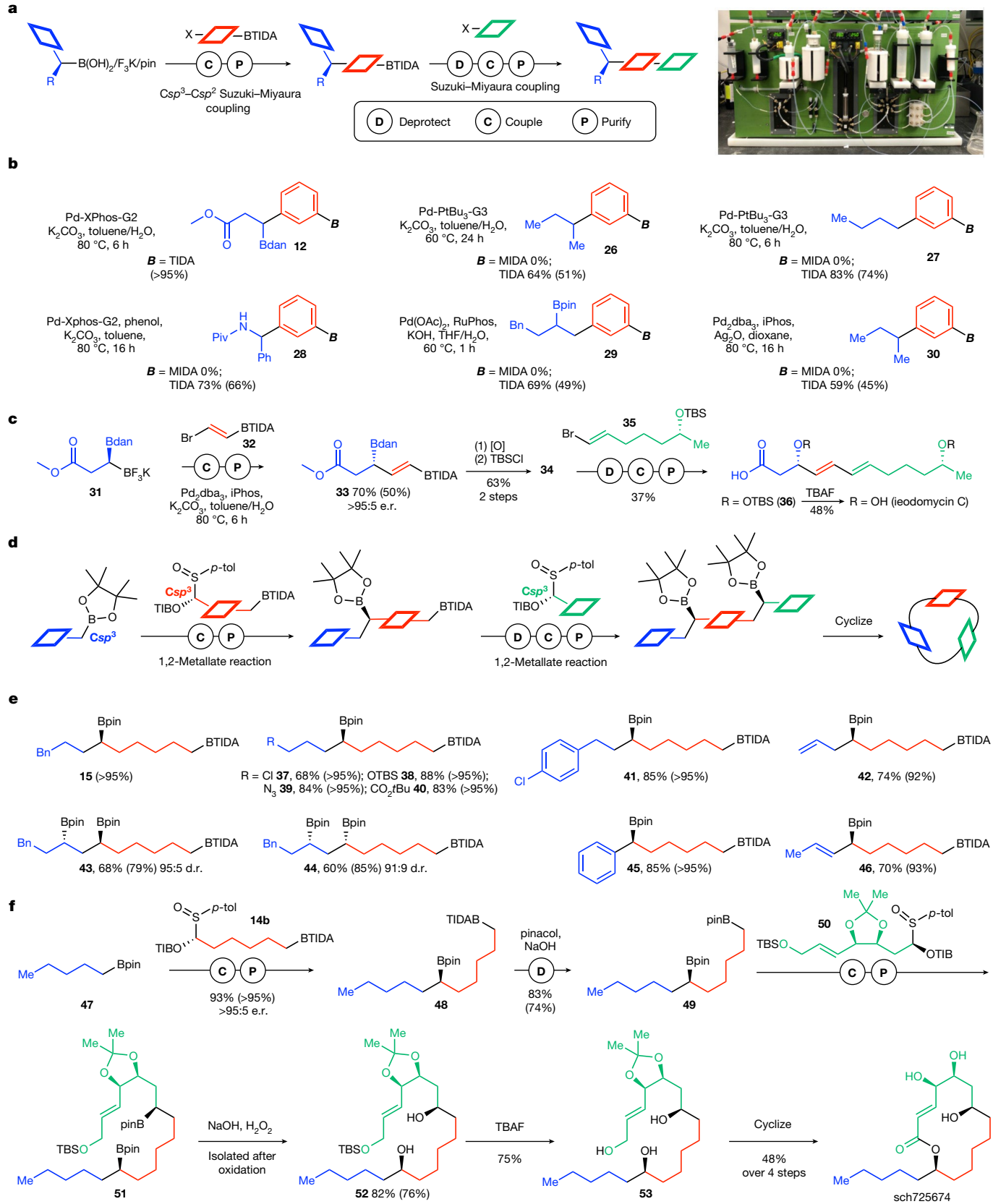

Fig. 4 | TIDA boronates enable automated assembly of Csp^3 boronate building blocks. a, TIDA boronates enable iterative Suzuki–Miyaura cross-coupling. **b**, Assembly of Csp^3 building blocks via Csp^3–Csp^2 Suzuki–Miyaura cross-coupling enabled by TIDA boronates. MIDA boronates universally provided no product. **c**, Automated stereospecific Csp^3 cross-coupling with TIDA boronate **32** enables lego-like synthesis of ieodomycin C. **d**, TIDA boronates enable iterative 1,2-metallate rearrangements. **e**, Assembly of Csp^3 building blocks via Csp^3–Csp^3 bond-forming 1,2-metallate rearrangements enabled by TIDA boronates. **f**, Sequential automated stereospecific Csp^3–Csp^3 bond formation using TIDA boronates enables lego-like synthesis of sch725674. For detailed experimental procedures see Supplementary Information. Yields for automated synthesis shown in parentheses. d.r., diastereoisomeric ratio.

50 to provide the core carbon scaffold of sch725674 (**52**) after oxidation of bisboronate **51**. Deprotection (TBAF, **53**), oxidative modification, macro-lactonization and final deprotection furnished sch725674 in only seven steps from bench-stable building blocks.

Online content

Any methods, additional references, Nature Research reporting summaries, source data, extended data, supplementary information, acknowledgements, peer review information; details of author contributions and competing interests; and statements of data and code availability are available at https://doi.org/10.1038/s41586-022-04491-w.

1. Trobe, M. & Burke, M. D. The molecular industrial revolution: automated synthesis of small molecules. *Angew. Chem. Int. Edn* **57**, 4192–4214 (2018).
2. Li, J. et al. Synthesis of many different types of organic small molecules using one automated process. *Science* **347**, 1221–1226 (2015).
3. Imao, D., Glasspoole, B. W., Laberge, V. S. & Crudden, C. M. Cross coupling reactions of chiral secondary organoboronic esters with retention of configuration. *J. Am. Chem. Soc.* **131**, 5024–5025 (2009).
4. Lehmann, J. W. et al. Axial shielding of Pd(II) complexes enables perfect stereoretention in Suzuki–Miyaura cross-coupling of Csp^3 boronic acids. *Nat. Commun.* **10**, 1263 (2019).
5. Mlynarski, S. N., Schuster, C. H. & Morken, J. P. Asymmetric synthesis from terminal alkenes by cascades of diboration and cross-coupling. *Nature* **505**, 386–390 (2013).
6. Ma, X., Murray, B. & Biscoe, M. R. Stereoselectivity in Pd-catalysed cross-coupling reactions of enantioenriched nucleophiles. *Nat. Rev. Chem.* **4**, 584–599 (2020).
7. Cherney, A. H., Kadunce, N. T. & Reisman, S. E. Enantioselective and enantiospecific transition-metal-catalyzed cross-coupling reactions of organometallic reagents to construct C–C bonds. *Chem. Rev.* **115**, 9587–9652 (2015).
8. Leonori, D. & Aggarwal, V. K. Lithiation-borylation methodology and its application in synthesis. *Acc. Chem. Res.* **47**, 3174–3183 (2014).
9. Sharma, H. A., Essman, J. Z. & Jacobsen, E. N. Enantioselective catalytic 1,2-boronate rearrangements. *Science* **374**, 752–757 (2021).
10. Casoni, G. et al. α-Sulfinyl benzoates as precursors to Li and Mg carbenoids for the stereoselective iterative homologation of boronic esters. *J. Am. Chem. Soc.* **139**, 11877–11886 (2017).
11. Bader, R. F. W., Slee, T. S., Cremer, D. & Kraka, E. Description of conjugation and hyperconjugation in terms of electronic distributions. *J. Am. Chem. Soc.* **105**, 5061–5068 (1983).
12. Bader, R. F. W. Ed. *Atoms in Molecules–A Quantum Theory* (Oxford Univ. Press, 1990).
13. Koritsanszky, T. S. & Coppens, P. Chemical applications of X-ray charge-density analysis. *Chem. Rev.* **101**, 1583–1628 (2001).
14. Fujita, K., Matsui, R., Suzuki, T. & Kobayashi, S. Concise total synthesis of (−)-myxalamide A. *Angew. Chem. Int. Edn* **51**, 7271–7274 (2012).
15. Seo, K.-B., Lee, I.-H., Lee, J., Choi, I. & Choi, T.-L. A rational design of highly controlled Suzuki–Miyaura catalyst-transfer polycondensation for precision synthesis of polythiophenes and their block copolymers: marriage of palladacycle precatalysts with MIDA-boronates. *J. Am. Chem. Soc.* **140**, 4335–4343 (2018).
16. Angelone, D. et al. Convergence of multiple synthetic paradigms in a universally programmable chemical synthesis machine. *Nat. Chem.* **13**, 63–69 (2021).
17. Lennox, A. J. J. & Lloyd-Jones, G. C. Selection of boron reagents for Suzuki–Miyaura coupling. *Chem. Soc. Rev.* **43**, 412–443 (2014).
18. Lovering, F., Bikker, J. & Humblet, C. Escape from flatland: increasing saturation as an approach to improving clinical success. *J. Med. Chem.* **52**, 6752–6756 (2009).
19. Worch, J. C. et al. Stereochemical enrichment of polymer properties. *Nat. Rev. Chem.* **3**, 514–535 (2019).
20. Gonzalaez, J. A. et al. MIDA boronates are hydrolysed fast and slow by two different mechanisms. *Nat. Chem.* **8**, 1067–1075 (2016).
21. Stephan, D. W. & Erker, G. Frustrated Lewis pairs: metal-free hydrogen activation and more. *Angew. Chem. Int. Edn* **49**, 46–76 (2010).
22. Mancilla, T. & Contreras, R. New bicylic organylboronic esters derived from iminodiacetic acids. *J. Organomet. Chem.* **307**, 1–6 (1986).
23. Mancilla, T., de los Ángeles Calixto Romo, M. & Delgado, L. A. Synthesis and characterization of (N→B) phenyl[*N*-alkyl-*N*-(2-alkyl)aminodiacetate-*O*,*O*′,*N*]boranes and phenyl[*N*-alkyl-*N*-(2-alkyl)aminodiacetate-*O*,*O*′,*N*]boranes. *Polyhedron* **26**, 1023–1028 (2007).
24. Wu, J. I.-C. & von Ragué Schelyer, P. Hyperconjugation in hydrocarbons: not just a "mild sort of conjugation". *Pure Appl. Chem.* **85**, 921–940 (2013).
25. Pophristic, V. & Goodman, L. Hyperconjugation not steric repulsion leads to the staggered structure of ethane. *Nature* **411**, 565–568 (2001).
26. Senderowitz, H., Golender, L. & Fuchs, B. New supramolecular host systems. 2. 1,3,5,7-Tetraoxadecalin, 1,2-dimethoxyethane and the gauche effect reappraised. Theory vs. experiment. *Tetrahedron* **32**, 9707–9728 (1994).
27. Hoffman, R. W., Hrovat, D. A. & Borden, W. T. Is hyperconjugation responsible for the "gauche effect' in 1-fluoropropane and other 2-subsituted-1-fluoroethanes? *J. Chem. Soc. Perkin Trans. 2* **12**, 1719–1726 (1999).
28. Scherer, W. et al. Valence-shell charge concentrations and electron delocalization in alkyllithium complexes: negative hyperconjugation and agnostic bonding. *Chem. Eur. J.* **8**, 2324–2334 (2002).
29. Hirschfeld, F. L. Bonded-atom fragments for describing molecular charge densities. *Theor. Chim. Acta* **44**, 129–138 (1977).
30. Jonas, V., Frenking, G. & Reetz, M. T. Comparative theoretical study of Lewis acid–base complexes of BH_3, BF_4, BCl_3, $AlCl_3$, and SO_2. *J. Am. Chem. Soc.* **116**, 8741–8753 (1994).
31. Skara, G., de Vleeschouwer, F., Geerlings, P., de Proft, F. & Pinter, B. Heterolytic splitting of molecular hydrogen by frustrated and classical Lewis pairs: a unified reactivity concept. *Sci. Rep.* **7**, 16024 (2017).
32. Schürmann, C. J. et al. Experimental charge density study on FLPs and a FLP reaction product. *Z. Kristallogr. Crystall. Mater.* **233**, 723–731 (2018).
33. Ullrich, M., Lough, A. J. & Stephan, D. W. Dihydrogen activation by $B(p\text{-}C_6F_4H)_3$ and phosphines. *Organometallics* **29**, 3647–3654 (2010).
34. Falivene, L. et al. Towards the online computer-aided design of catalytic pockets. *Nat. Chem.* **11**, 872–879 (2019).
35. Beak, P. & Carter, L. G. Dipole-stabilized carbanions from esters: α-oxo lithiations of 2,6-substituted benzoates of primary alcohols. *J. Org. Chem.* **46**, 2363–2373 (1981).
36. Landry, M. L., Hu, D. X., McKenna, G. M. & Burns, N. Z. Catalytic enantioselective dihalogenation and the selective synthesis of (−)-deschloromytilipin A and (−)-danicalipin A. *J. Am. Chem. Soc.* **138**, 5150–5158 (2016).
37. Mojid Mondol, M. A. et al. Ieodomycins A–D, antimicrobial fatty acids from a marine *Bacillus* sp. *J. Nat. Prod.* **74**, 1606–1612 (2011).
38. Blakemore, P. R., Marsden, S. P. & Vater, H. D. Reagent-controlled asymmetric homologation of boronic esters by enantioenriched main-group chiral carbenoids. *Org. Lett.* **8**, 773–776 (2006).
39. Roesner, S., Blair, D. J. & Aggarwal, V. K. Enantioselective installation of adjacent tertiary benzylic stereocentres using lithiation-borylation-protodeboronation methodology. Application to the synthesis of bifluranol and fluorohexestrol. *Chem. Sci.* **6**, 3718–3723 (2015).
40. Yang, S.-W. et al. Structure elucidation of sch725674 from *Aspergillus* sp. *J. Antibiot.* **58**, 535–538 (2005).
41. Fawcett, A. et al. Regio- and stereoselective homologation of 1,2-bis(boronic esters): stereocontrolled synthesis of 1,3-diols and sch725674. *Angew. Chem. Int. Edn* **55**, 14663–14667 (2016).
42. Momma, K. & Izumi, F. VESTA 3 for three-dimensional visualization of crystal, volumetric and morphology data. *J. Appl. Crystallogr.* **44**, 1272–1276 (2011).
43. O'Brien, N. J. et al. Synthesis, structure and reactivities of pentacoordinated phosphorus-boron bonded compounds. *Eur. J. Inorg. Chem.* **20**, 1995–2003 (2020).
44. Uno, B. E., Gillis, E. P. & Burke, M. D. Vinyl MIDA boronate: a readily accessible and highly versatile building block for small molecule synthesis. *Tetrahedron* **65**, 3130–3138 (2009).
45. Ma, Y. et al. Radical C–N borylation of aromatic amines enabled by a pyrylium reagent. *Chem. Eur. J.* **26**, 3738–3743 (2020).
46. Neuvonen, H., Neuvonen, K., Koch, A., Kleinpeter, E. & Pasanen, P. Electron-withdrawing substituents decrease the electrophilicity of the carbonyl carbon. An investigation with the aid of ^{13}C NMR chemical shifts, ν(C=O) frequency values, charge densities, and isodesmic reactions to interpret substituent effects on reactivity. *J. Org. Chem.* **67**, 6995–7003 (2002).
47. Aspin, S., Goutierre, A.-S., Larini, P., Jazzar, R. & Baudoin, O. Synthesis of aromatic α-aminoesters: palladium-catalyzed long-range arylation of primary Csp^3-H bonds. *Angew. Chem. Int. Edn* **51**, 10808–10811 (2012).
48. Li, G., Ji, C.-L., Hong, X. & Szostak, M. Highly chemoselective, transition-metal-free transamidation of unactivated amides and direct amidation of alkyl esters by N-C/O-C cleavage. *J. Am. Chem. Soc.* **141**, 11161–11172 (2019).
49. Xie, X. & Stahl, S. S. Efficient and selective Cu/nitroxyl-catalyzed methods for aerobic oxidative lactonization of diols. *J. Am. Chem. Soc.* **137**, 3767–3770 (2015).
50. Yamamato, Y., Nemoto, H., Kikuchi, R., Komatsu, H. & Suzuki, I. A conformationally rigid acyclic molecule. *J. Am. Chem. Soc.* **112**, 8598–8599 (1990).
51. Ueki, Y., Ito, H., Usui, I. & Breit, B. Formation of quaternary carbon centers by highly regioselective hydroformylation with catalytic amounts of a reversibly bound directing group. *Chem. Eur. J.* **17**, 8555–8558 (2011).

Data availability

X-ray crystal structure data are available free of charge on the Cambridge Crystallographic Data Centre under the following accession numbers: 4-bromophenylboronic acid MIDA ester **1c**: structure 2087874, multipole refinement 2087875; 4-bromophenylboronic acid TIDA ester **20**: structure 2087872, multipole refinement 2087873; 3-bromophenylboronic acid dimethyl-MIDA ester **SI-10**: structure 2087648; ethynylboronic acid TIDA ester **SI-47**: structure 2087715; *cis*-2-bromovinylboronic acid TIDA ester **SI-49**: structure 2087714; *trans*-2-bromovinylboronic acid TIDA ester **32**: structure 2087712; sulfinyl benzoate *anti*-**SI-25**: structure 2087716; TIDA anhydride: structure 2120500. All other data are available in the main text or supplementary materials.

Acknowledgements We thank F. Sun and H. Yao at the UIUC Mass Spectrometry Facility, D. Olson, L. Zhu and N. Duay at the School of Chemical Sciences NMR Laboratory at UIUC for NMR services, and members of the Burke laboratory for discussions related to this project. The Bruker 500 MHz NMR spectrometer was obtained with the financial support of the Roy J. Carver Charitable Trust, Muscatine, Iowa, USA. D.J.B. thanks the Damon-Runyon Cancer Research Foundation for additional support during the COVID-19 pandemic. S. Denmark is acknowledged for manuscript review. We thank P.-J. Chen, Y. Tong, A. Blake, H. Auby and D. Szczepankiewicz for technical assistance. Support was provided by the following sources: M.D.B.: NIH (GM118185), NSF (CHE-1955838); D.J.B.: Illini 4000 Fellow of the Damon-Runyon Cancer Research Foundation DRG-2290-17; S.C.: ACS Division of Organic Chemistry Summer Undergraduate Research Fellowship, Henry Luce Foundation and the Illinois Scholars Undergraduate Research Program; M.B.T.: Erwin Schrödinger Post-Doctoral Fellow, Austrian Science Fund (FWF) (J3960-N34).

Author contributions The project was designed by D.J.B., M.J.S. and M.D.B. Experimental work was conducted by D.J.B., S.C., M.T., D.M.K., H.M.S.H., R.L.H., S.G.B., T.J.W., W.W., V.M., M.J.S., R.W.P., G.F.M., A.M.E.P.R. and D.L.G. Automated synthesis experiments were performed by D.J.B., M.T. and H.M.S.H with guidance from R.L.H. and S.G.B. Crystallographic data were collected by T.J.W. and D.L.G. Multipole structural refinements were performed by T.J.W. Small-molecule synthesis machines were designed, constructed and finalized by R.L.H., S.G.B., A.L.G. and M.D.B. D.J.B. and M.D.B. wrote the manuscript.

Competing interests The University of Illinois has filed patent applications related to MIDA and TIDA boronates. M.D.B. is a founder, shareholder and consultant for REVOLUTION Medicines.

Additional information
Supplementary information The online version contains supplementary material available at https://doi.org/10.1038/s41586-022-04491-w.
Correspondence and requests for materials should be addressed to Daniel J. Blair or Martin D. Burke.
Peer review information *Nature* thanks the anonymous reviewers for their contribution to the peer review of this work.

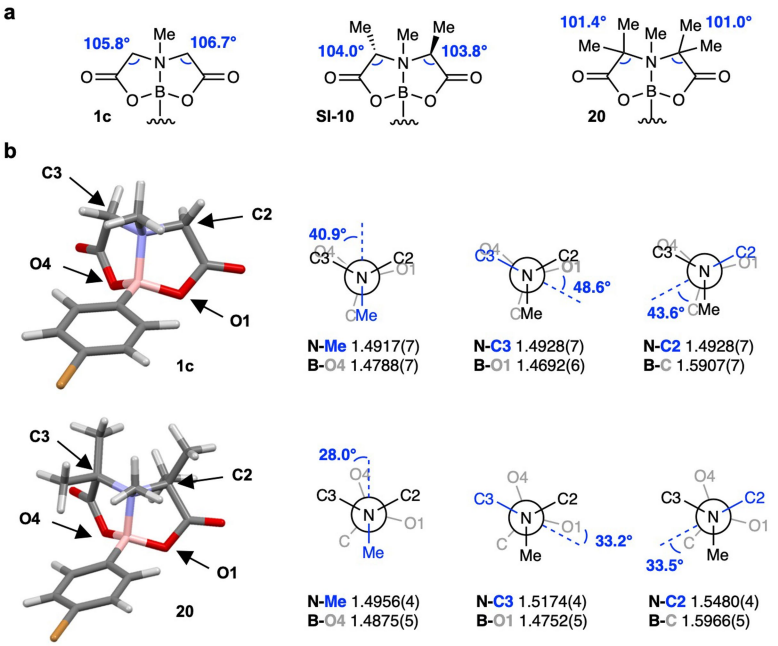

Extended Data Fig. 1 | Structural consequences of backbone substitution on iminodiacetic acid boronates. a, Internal angle compression from MIDA **1c** to dimethyl-MIDA **SI-10** to TIDA **20** suggest thermodynamic Thorpe–Ingold effects might further support hyperconjugative interactions by rigidifying the iminodiacetic acid cage of TIDA. **b**, Increases in nitrogen attached donor and boron attached acceptor bond lengths for TIDA **20** compared to MIDA **1c** support hyperconjugative transfer of electron density along the N-B bond (lengths in Å).

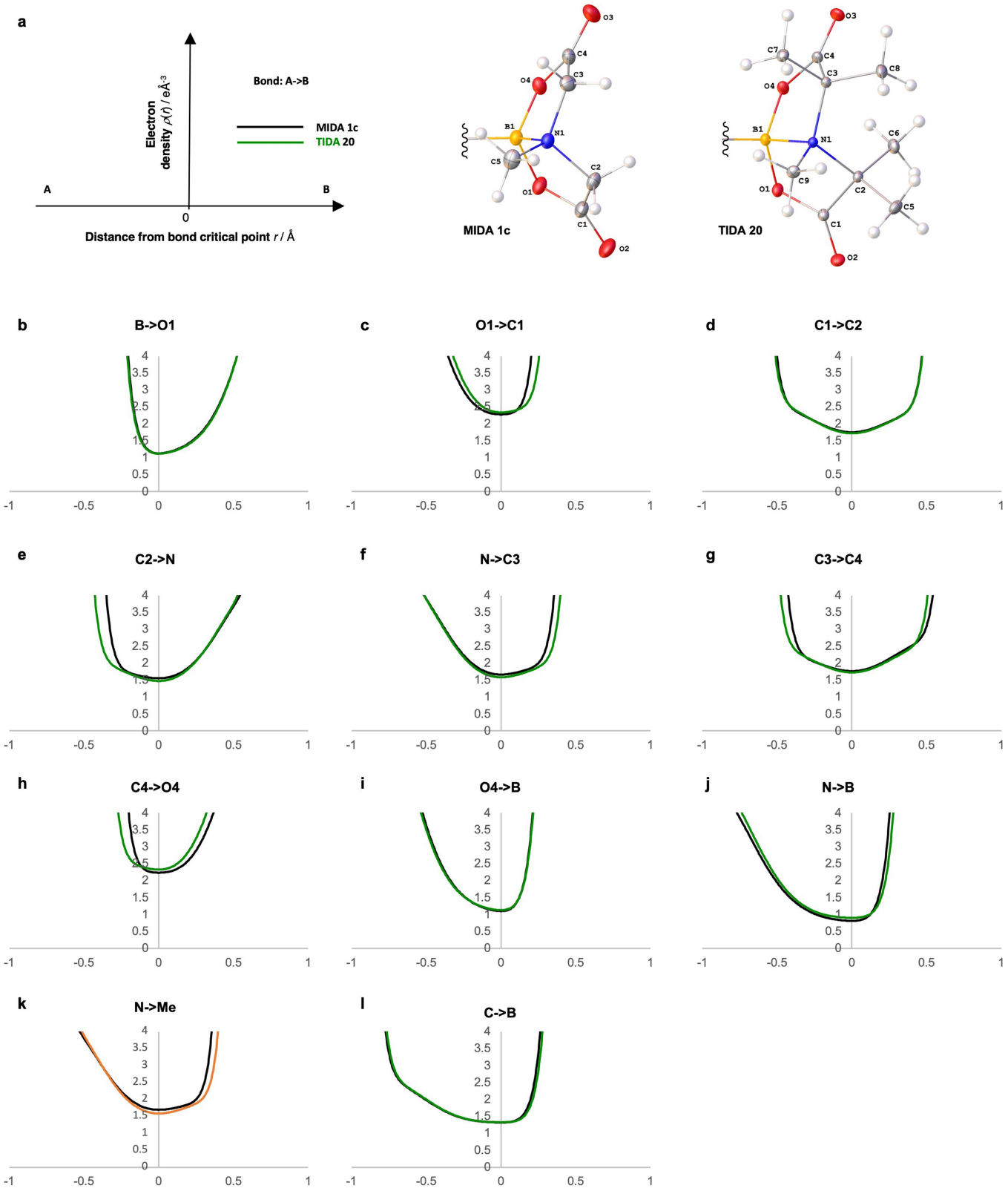

Extended Data Fig. 2 | Bond path total electron density for MIDA boronate 1c and TIDA boronate 20. a, Legend and numbered molecular structures. **b**–**i** Follow anticlockwise around the iminodiacetic acid cage. **j**–**l**, The N-B, N-Me, and C-B bonds are also included. The maximum displayed value of the electron density (*y*-axis) is capped at 4 eA^{-3} to best capture the interatomic bonding region.

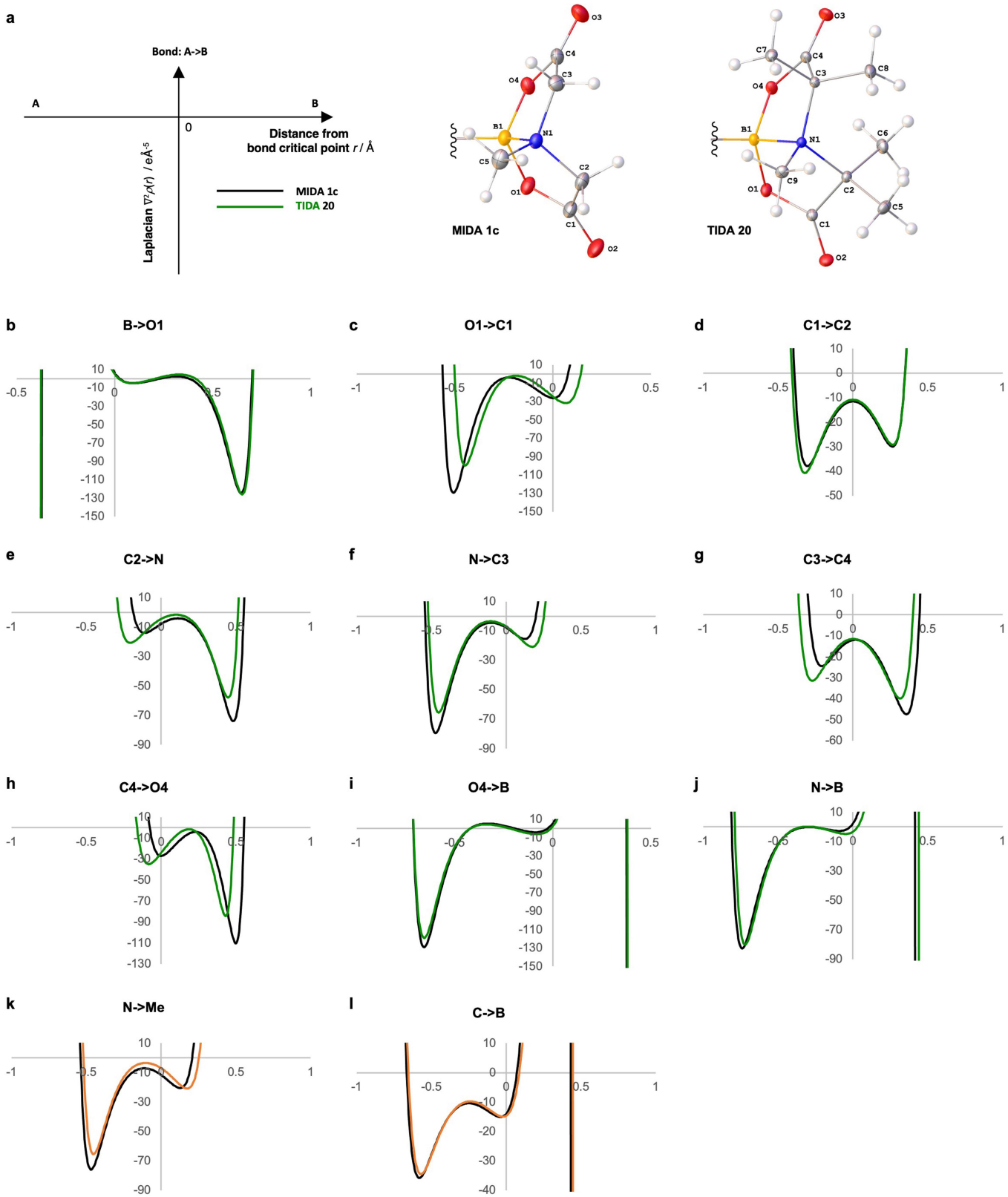

Extended Data Fig. 3 | Bond path Laplacian profiles comparing MIDA boronate 1c and TIDA boronate 20. a, Legend and labelled structures. **b**–**i** Follow an anticlockwise path around MIDA **1c** and TIDA **20** as well as the N-B, N-Me, and C-B bonds (**j**–**l**).

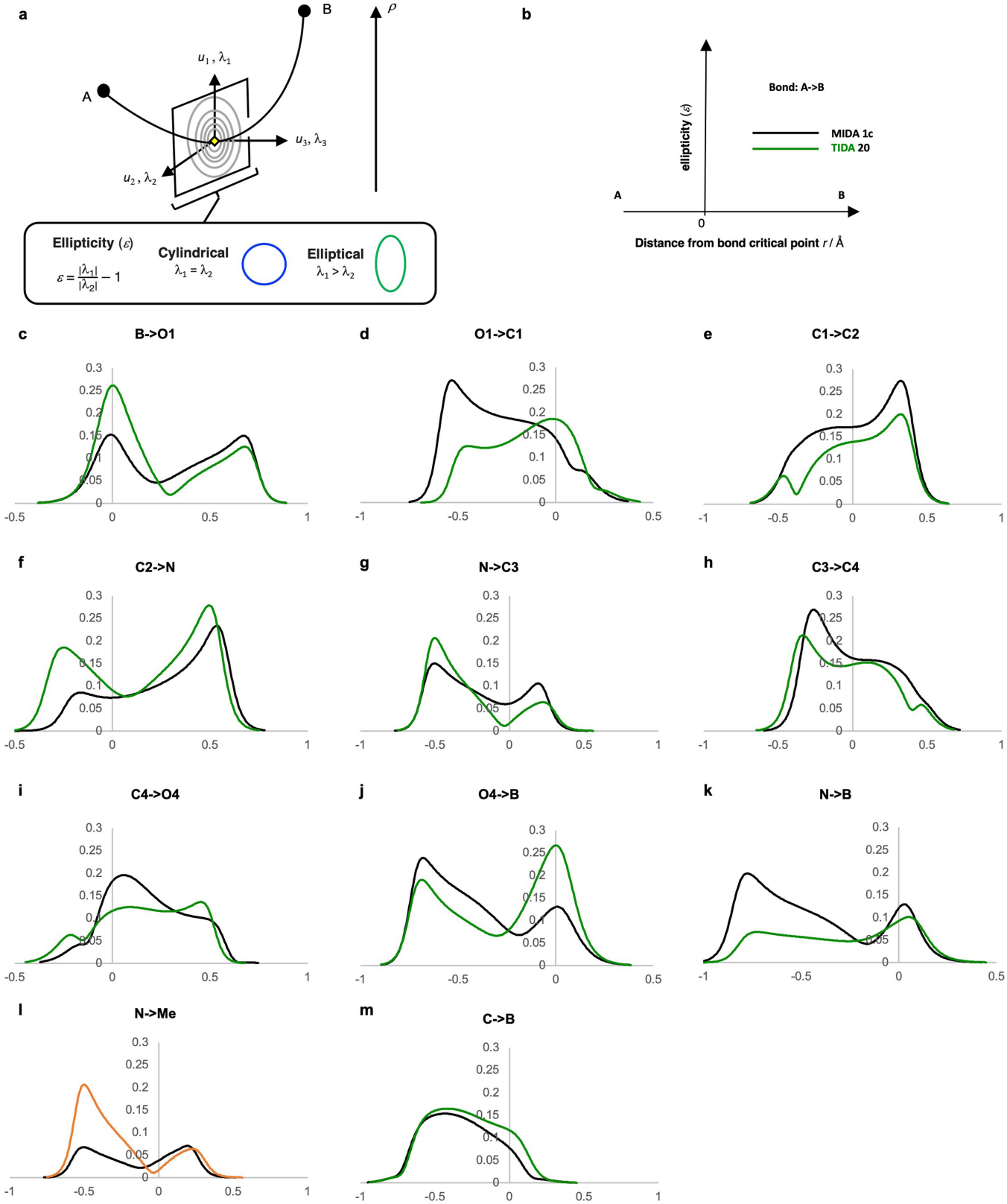

Extended Data Fig. 4 | Bond path ellipticity profiles for MIDA boronate 1c and TIDA boronate 20. a, Schematic representation of ellipticity (ε), which reflects an increase in directionality of electron density and is characteristic of increased π-character. **b**, Legend for sections **c**–**m**. Pronounced changes in ellipticity can be seen for TIDA boronate **20** compared to MIDA boronate **1c** particularly for the N-C2/3 (**f**, **g**), B-O1/4 (**c**, **j**), and N-B bonds, which are consistent with observations of redistributions of electron density around the N-B bond (see Fig. 3a, b). Ellipticity profiles (**c**–**j**) follow an anticlockwise path around the iminodiacetic acid rings of **1c** and **20** starting with B-O1 (**c**) and ending with O4-B (**j**). Profiles for the N-B, N-Me, and C-B bonds (**k**–**m**) are also included.

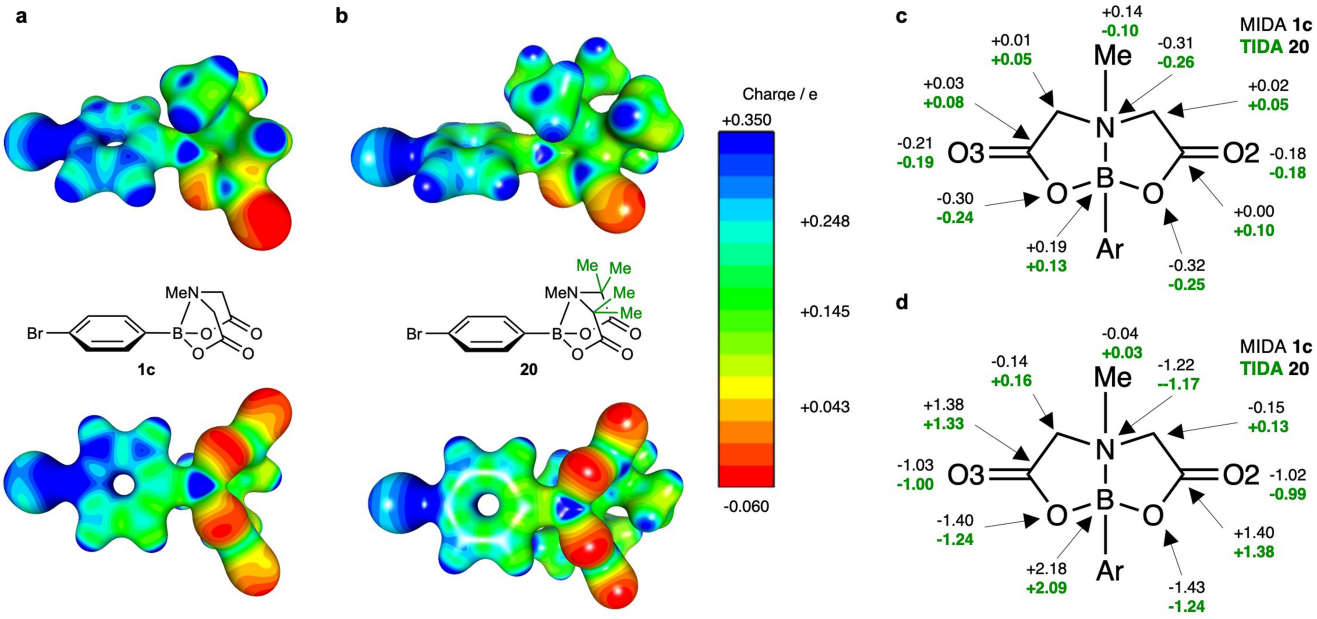

e

	δ_C (C=O) acetone-d_6		δ_B acetone-d_6	
	MIDA	TIDA	MIDA	TIDA
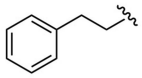	168.9[43]	175.1	12.9[43]	10.5
	169.0[44]	175.1	12.8	10.6
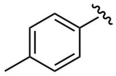	169.3[45]	175.7	11.8[45]	9.3
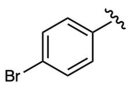	169.2[45]	175.3	11.4[45]	9.3

f

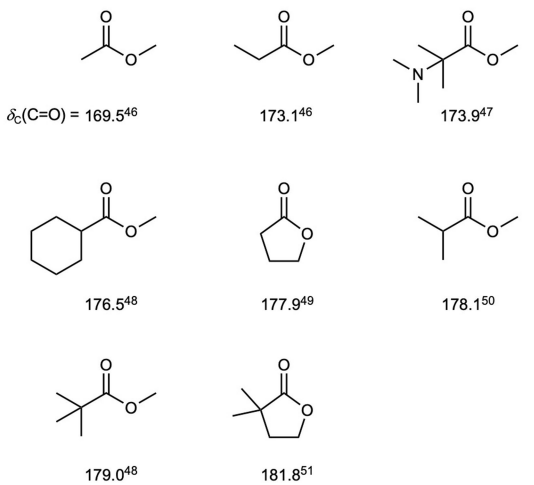

Extended Data Fig. 5 | Charge analysis of MIDA boronate 1c and TIDA boronate 20. a, Electrostatic potential surface for MIDA **1c**, showing side on and bottom perspectives. **b**, Electrostatic potential surface for TIDA **20**, showing side on and bottom perspectives. **c**, Stockholder charges comparing MIDA **1c** (black) and TIDA **20** (green), values shown are in electrons. **d**, Integrated charge comparing MIDA **1c** (black) and TIDA **20** (green), values shown are in electrons. TIDA backbone methyl groups were omitted for clarity on the charge plots. **e**, A downfield shift for TIDA boronates carbonyl carbons indicates a net electron depletion relative to MIDA boronates. Similarly, there is an up-field shift for the boron atoms in TIDA boronates relative to MIDA boronates indicating increased boronate complex-like character and elevated electronic shielding[43–45]. **f**, Trends in ^{13}C NMR carbonyl chemical shifts in $CDCl_3$ on sequential substitution of the α-carbon with methyl groups and/or lactone formation and/or addition of an α-dimethylamino group are provided for comparison[46–51].

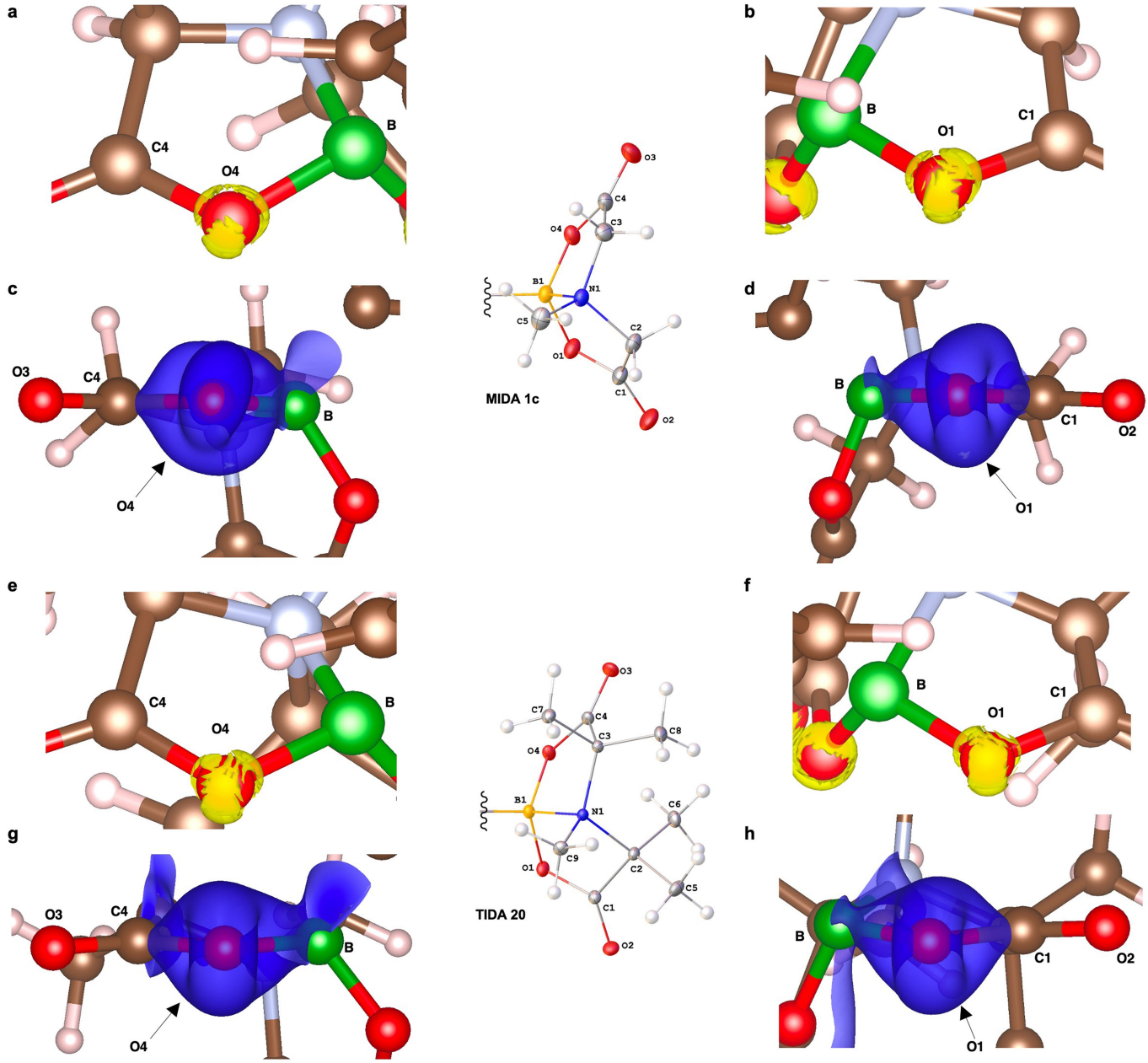

Extended Data Fig. 6 | Laplacian and electron density isosurfaces support redistributed density around the O4-B-O1 linkage of TIDA 20. a, The Laplacian at isosurface value -80 eA^{-5} (shown in yellow) for MIDA **1c** indicates an isolated valence shell charge concentration (VSCC) at O4 (i.e. minimal lone-pair interactions). **b**, Unlike at O4 the Laplacian at O1 for MIDA **1c** reveals coalescence of lone-pair VSCC and the O1-C1 VSCC, pointing toward interaction between O1 and C1 (the adjacent carbonyl). **c**, End-on view of deformation density (isosurface value of 0.0034 eA^{-3} in blue) down O4 in MIDA **1c** provides further evidence for charge localization at O4. **d**, In contrast to O4 the end-on view of deformation density down O1 for MIDA **1c** reveals the electron distribution along B-O1-C1, favours O1-C1. **e**, The Laplacian of TIDA **20** reveals interaction between lone-pair VSCC and both C4-O4/O4-B VSCCs. **f**, In contrast to MIDA **1c** the lone-pair VSCC of TIDA **20** at O1 coalesces with the B-O1 VSCC and not the O1-C1 VSCC. **g**, **h**, Consistent with these changes in VSCCs, deformation density at O4 (**g**) and O1 (**h**) for TIDA **20** supports electronic redistribution about the C4-O4-B-O1-C1 network compared to MIDA **1c**. Prepared using VESTA 3 (ref. [42]).

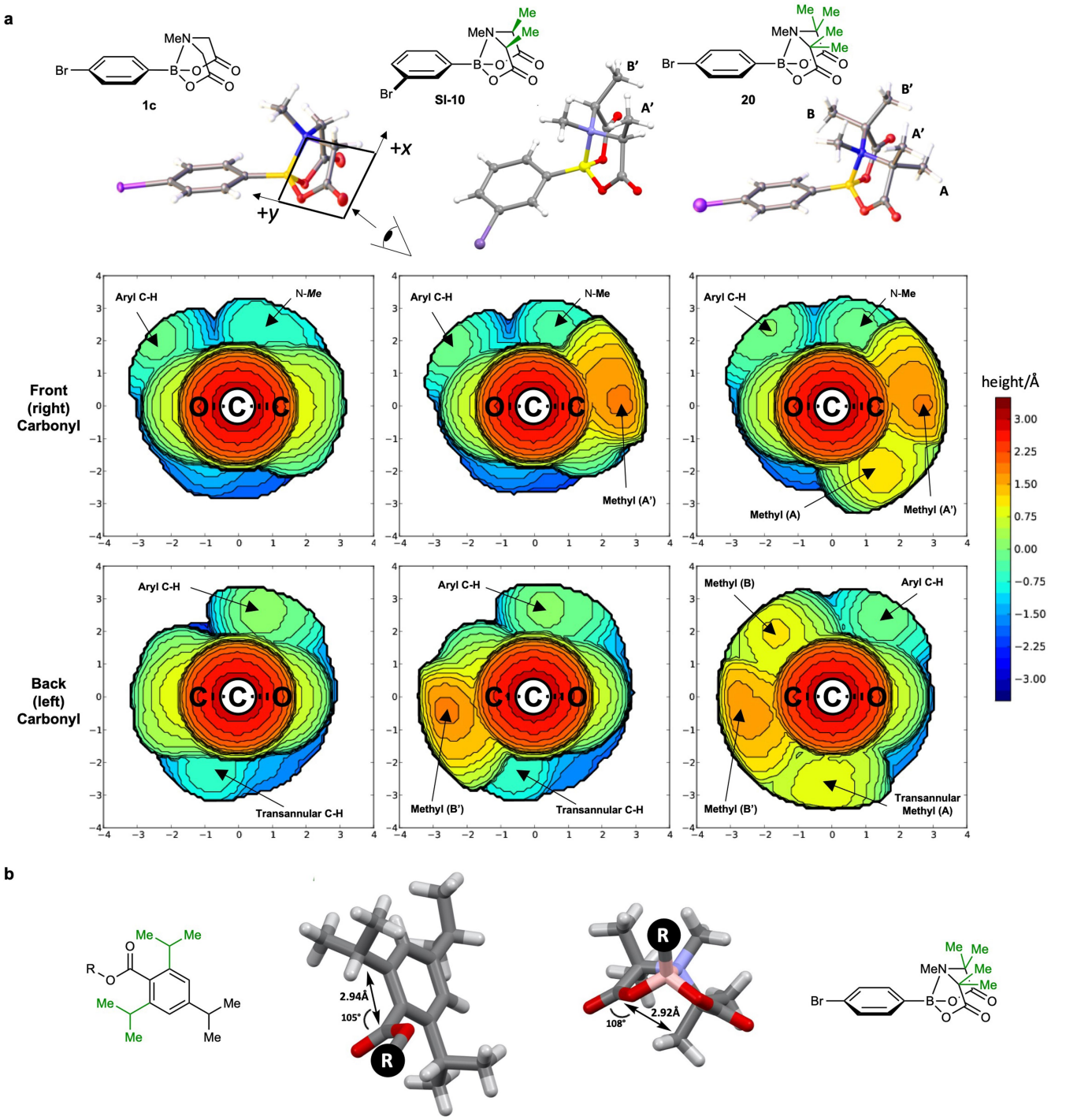

Extended Data Fig. 7 | Robust steric shielding suppresses carbonyl attack on TIDA boronates. a, Topological steric maps[34] of the plane perpendicular to the carbonyl carbons enable comparison of MIDA (**1c**), dimethyl-MIDA (**SI-10**), and TIDA (**20**). MIDA boronates (left column) experience minimal steric shielding, and methyl groups introduced in dimethyl-MIDA (A' and B') occupy pseudo-equatorial positions, minimally impacting carbonyl approach (centre column). The two additional methyl groups in TIDA (A and B) occupy pseudo-axial positions and establish transannular steric shielding interactions between A and the carbonyl on the opposite side of the TIDA framework (right column). Additionally, A and B shield their adjacent carbonyls towards approach at the Burgi-Dunitz angle. **b**, The transannular influence of methyl group A mirrors that of Beak-type 2,4-6-triisopropyl benzoates which are resistant to carbon centred nucleophiles.

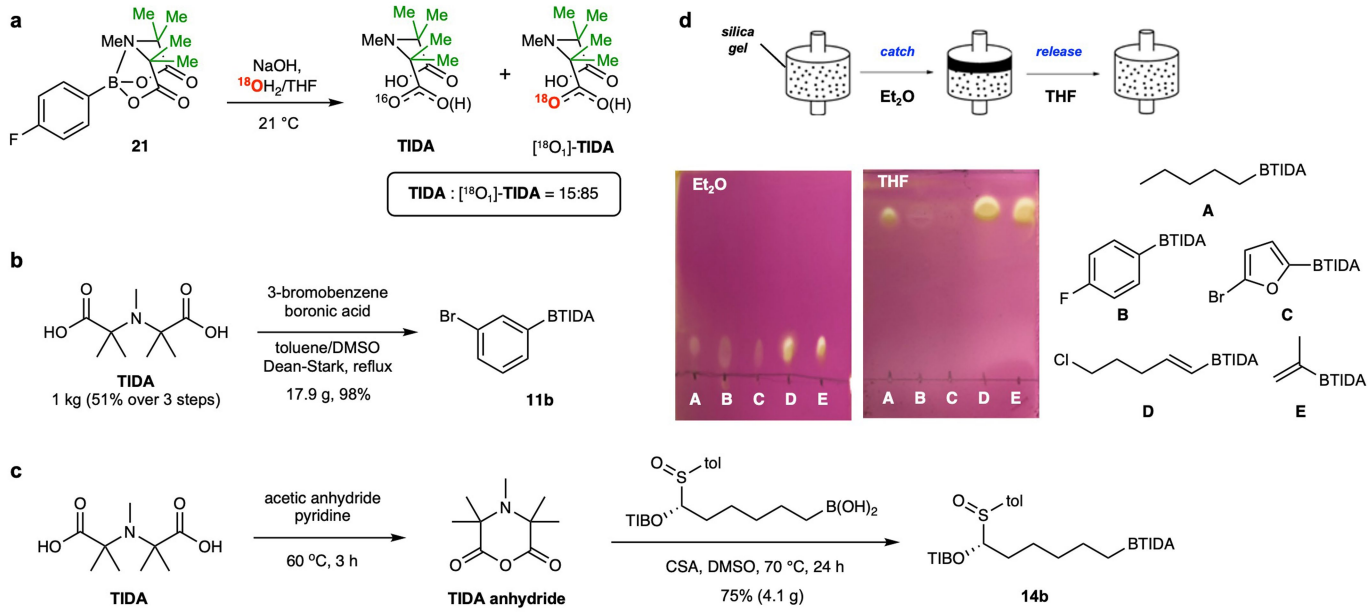

Extended Data Fig. 8 | TIDA boronates retain all required properties to enable generalized automated synthesis. a, TIDA boronate **21** is hydrolysed by NaOH primarily *via* the ester hydrolysis mechanism. **b**, TIDA ligand and TIDA boronates can be prepared on scale. **c**, TIDA anhydride provides an alternative method to prepare TIDA boronates. **d**, TIDA boronates possess a binary affinity for silica gel, agnostic of the attached carbon fragment. They are minimally mobilized in Et_2O and rapidly eluted in THF, enabling generalized and automatable catch-and-release purification. tol, *para*-toluene.

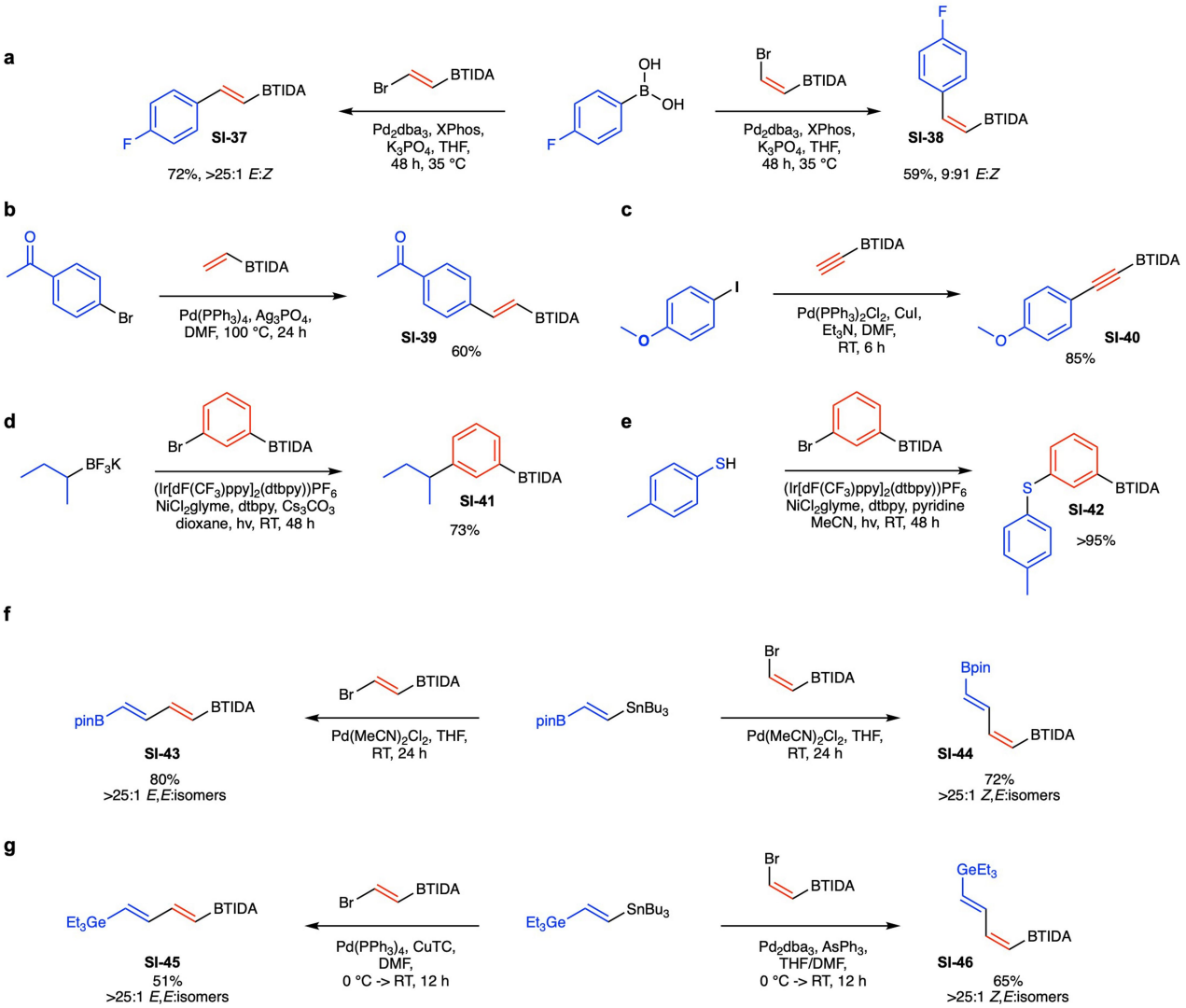

Extended Data Fig. 9 | TIDA boronates tolerate a diverse range of cross-coupling chemistry. a, Suzuki–Miyaura cross-coupling. **b**, Heck coupling. **c**, Sonogashira coupling. **d**, Photochemical Suzuki–Miyaura cross-coupling. **e**, Photochemical thioetherification. **f**, Stille coupling leading to bis-borylated dienes. **g**, Stille coupling leading to germylated dienes.

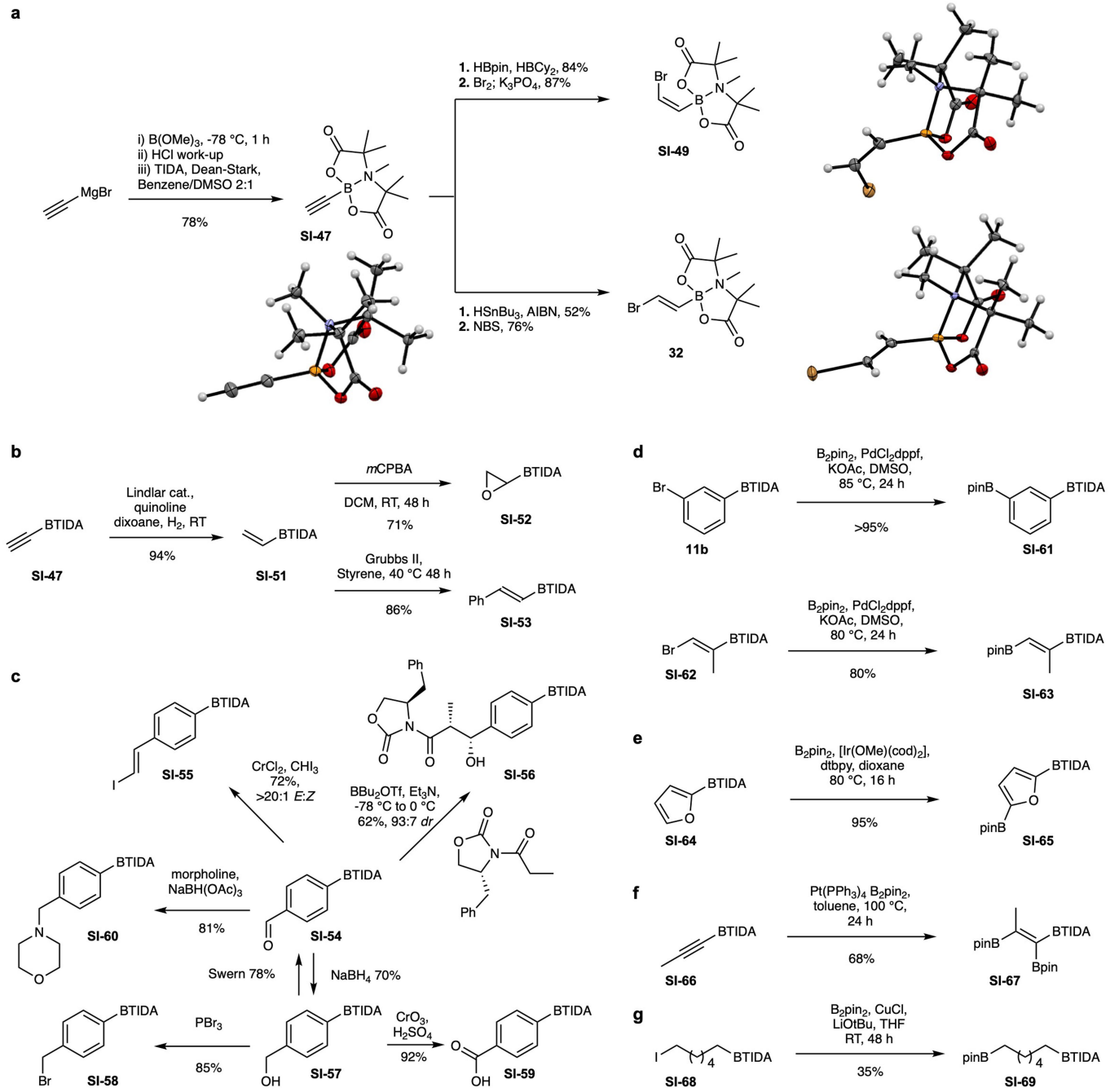

Extended Data Fig. 10 | Functional group interconversion of TIDA boronate building blocks. a, Ethynylboronic acid TIDA ester is readily converted into *E*- and *Z*- 2-bromovinylboronic acid TIDA esters with excellent stereocontrol. Images of X-ray crystal structures shown inset. **b**, Reduction of ethynylboronic acid TIDA ester furnishes vinylboronic acid TIDA ester which participates in epoxidation and Grubbs metathesis. **c**, Common functional group interconversion reactions are well tolerated by TIDA including oxidation, reduction, halogenation, reductive amination, Evans aldol and Takai olefination. **d**–**g**, A wide range of borylation chemistries are tolerated by TIDA boronates to produce mono-protected polyborylated building blocks, including Miyaura (**d**), C-H borylation (**e**), diboration (**f**), and copper catalysed borylation (**g**).